



# VCU

Virginia Commonwealth University  
VCU Scholars Compass

---

Theses and Dissertations

Graduate School


---

2017

## Quantitative Analysis and Process of High Speed Live Cell Interferometry Measurements

Daniel Guest  
*Virginia Commonwealth University*

Follow this and additional works at: <https://scholarscompass.vcu.edu/etd>

 Part of the [Biological and Chemical Physics Commons](#), [Engineering Physics Commons](#), and the [Optics Commons](#)

© The Author

---

Downloaded from

<https://scholarscompass.vcu.edu/etd/4843>

This Thesis is brought to you for free and open access by the Graduate School at VCU Scholars Compass. It has been accepted for inclusion in Theses and Dissertations by an authorized administrator of VCU Scholars Compass. For more information, please contact [libcompass@vcu.edu](mailto:libcompass@vcu.edu).

# **Quantitative Analysis and Process of High Speed Live Cell Interferometry Measurements**

A thesis submitted in partial fulfillment of the requirements for the  
degree of Master of Science at Virginia Commonwealth University.

by

Daniel Carter Guest Jr.

Master of Science in Physics and Applied Physics

Director: Dr. Jason Reed,

Assistant Professor, Physics Department

Virginia Commonwealth University

Richmond, Virginia

May, 2017

# Table of Content

List of Figures .....	i
List of Abbreviations.....	ii
Abstract.....	iii
Introduction.....	1
Methods.....	3
General.....	3
Laser Focus Technique .....	10
Electrical Circuitry/Hardware Interfacing .....	14
Validation .....	21
PID Error .....	21
Effect of temperature .....	23
Mast Cell Experiment .....	24
Design of experiment.....	24
Results .....	26
Possible addition to experiment.....	30
Conclusion .....	31
Appendix A .....	32
Bibliography.....	36

# List of Figures

Figure (1) Plate Diagram .....	3
Figure (2) Relative Objective Position for Typical Scan .....	5
Figure (3) Camera Technique.....	7
Figure (4) Ray Diagram of Laser Focus System.....	10
Figure (5) Objective Ramp vs. QPD .....	12
Figure (6) Layout of Circuit .....	14
Figure (7) Hardware Configuration.....	15
Figure (8) Instrumentation Amplifier Diagram.....	19
Figure (9) Histograms of Error .....	21
Figure (10) Mast Cell Mass Track .....	26
Figure (11) Ramp @ 40x .....	27

## List of Abbreviations

high speed live cell interferometry measurements (HSLCI)

quadri-wave lateral shearing interferometer (QWLSI)

quadrant photodiode(QPD)

frames per second (fps)

Virginia Commonwealth University (VCU)

proportional–integral–derivative (PID)

capture computer (CC)

processing computer (PC)

optical path difference(OPD)

analog to digital converter (ADC)

digital to analog convertor (DAC)

dinitrophenylated human serum albumin (DNP-HSA)

# **Abstract**

## QUANTITATIVE ANALYSIS AND PROCESS OF HIGH SPEED LIVE CELL INTERFEROMETRY MEASUREMENTS

By Daniel Guest, MS Applied Physics

A thesis submitted in partial fulfillment of the requirements for the degree of Master of Science at Virginia Commonwealth University.

Virginia Commonwealth University, 2017.

Major Director: Dr. Jason Reed, Assistant Professor, Physics Department.

The application of auto focus, using an optical beam deflection technique, to existing live cell interferometry measurements was developed and examined. The benefit to relevant experiments, currently being performed, is shown as well as its performance across various magnifications. Enough information is given so that the system can be reproduced to fit any end users needs.

# Introduction

This paper will discuss the overall function and structure that was necessary to perform high speed live cell interferometry(HSLCI) measurements. Live cell interferometry techniques allow the user to measure the phase shift of incident light through cells, which directly correlates to the cells dry mass. This label free technique is non-invasive and accurate enough to give detailed reports on the growth of the cells during multiple cell cycles over multiple days. This is useful because dry mass can be a direct result of biosynthetic and degradative processes within a cell, giving a precise metric of cell size during a response to drug treatments or cell death. Because this technique gives a resolution much smaller than individual components of the cell, the distribution of mass through out the cell can be easily rendered as a function of time.(Reed, J. et al. 2011)

Previously the dry mass of two cell samples with a 4x4 imaging grid of each sample were examined using a quadri-wave lateral shearing interferometer (QWLSI) with z-ramp based focus. Now, with laser autofocus, using the same interferometry technique, we can examine three times the sampling grid per sample in a fraction of the time. This new technique allows for 24-48 samples in parallel to be measured from 1-72 hours continuously.

Autofocus helps the user to overcome any problems due to mechanical instability, changes in glass thickness, and thermal expansion. Previously, a contrast metric was

used and a frame/stage position was found as best focus. This focusing process took approximately eight seconds per image. The autonomous feature of the new set-up allows the sampling stage to move continuously, while currently acquiring four frames per second (fps), no matter the topography of the sampling surface. The laser auto focus uses an optical beam deflection position measurement that could be spliced into the existing optical pipeline without any major changes.

To help show functional capability of the autofocus system, there will be discussion on an experiment done in collaboration with the Ryan Lab in the Biology Department at Virginia Commonwealth University (VCU). The Ryan Lab is focused on cellular and molecular immunology and works with primary mast cells that are derived from Black 6 mice. The previous configuration was able to successfully show a decrease in mass, from degranulation, of 5-30% on a single cell basis.

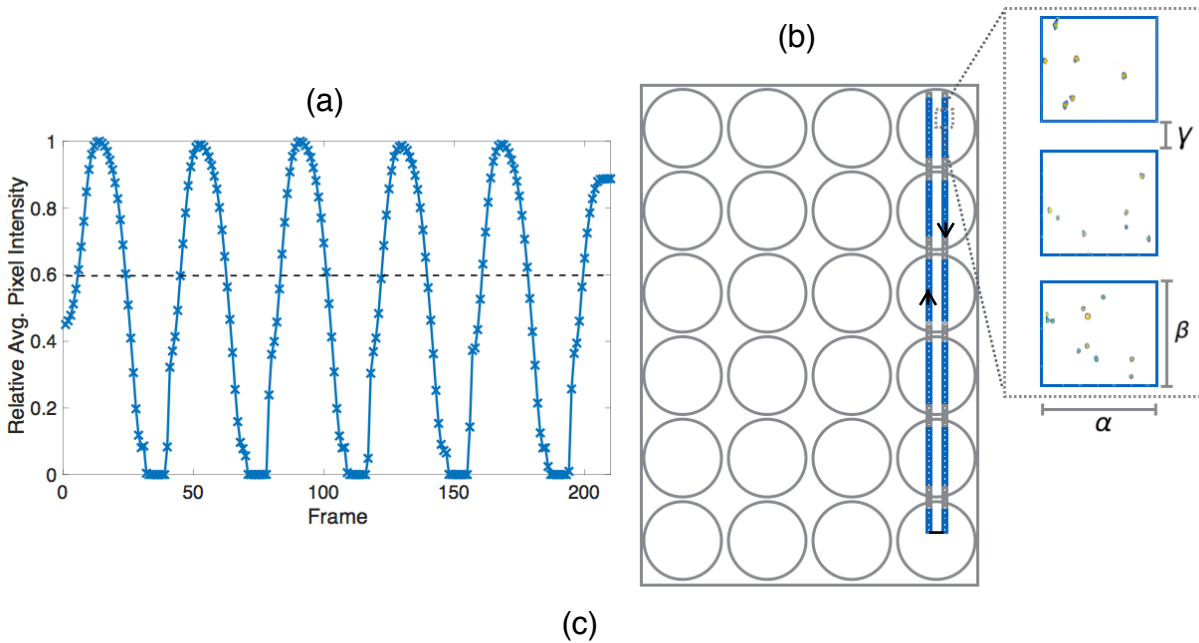
The next step in the current collaboration was to see how long it took for the cells to regain their mass. The current theory is that it takes roughly 48 to 72 hours after they degranulate. This proved problematic for the 4x4 imaging grid because a mast cell does not stick to the surface of the well and can be lost after a few frames of imaging. It was predicted that the increase in imaging grid and increase in sampling wells would give enough cells to average as the cells swept across each frame from loop to loop. This was proved successful as will be described later in the paper.



# Methods

## General

The largest problem with the previous LCI setup was the time it took to insure the camera was in focus. Ideally, if minimal time lapse between frames is desired, the stage needs to run continuously. This would then require that the objective stay the desired distance



	10x	20x	40x
$\alpha(\mu m)$	1020	510	255
$\beta(\mu m)$	720	360	180
$\gamma(\mu m)$	-220*	140	320

### Figure (1) Plate Diagram

(a) The normalized average pixel intensity of each interferogram, marked by  $\times$  is plotted. The threshold for acceptable frames is marked by the dashed line. (b) The 24 well plate which measures approximately 12 cm long by 8 cm wide can be seen. The linear scan of each video file and location of each frame is shown for the far right column of wells. A series of three images of mast cells @40x are shown with each corresponding measurement. (c) Dimension of variables in (b). \* indicates an overlap of images

away from the sample, even if the well shape/thickness/height changed. This requires a feedback loop that can monitor the distance between the objective and sample and make any necessary changes to ensure it remains constant.

Given an optical set-up was already in place, an optical beam deflection provides necessary sensitivity ( $\sim 100nm$ ) and speed ( $< 100Hz$ ). Using a series of beam splitters, a laser beam can be reflected off of the glass to water interface where the cells are sitting in suspension. Looking at Figure (4) one can see where a change in distance between the objective and surface gives a change in distance from the beam going out of the objective to the beam re-entering the objective. This signal was then focused down to a sensor that is a desired length away. The sensor is a quadrant photodiode (QPD) where the intensity/position of the laser can be mapped to a dynamic analog voltage. Once this signal is conditioned, it serves as the input to the feedback loop. Since the distance between sample and objective is the key factor, the output of the feedback loop is accomplished by attaching the objective to a one-dimensional piezo stack with a range of 100 microns. The control of this feedback loop was accomplished using a stand alone, low-cost microprocessor, Arduino Nano.

The control loop feedback used is a form of a proportional–integral–derivative (PID) controller where an error value is continuously calculated as the difference between a set-point and the measured process variable. Only the first two terms are currently being used, therefore the sum of the P and I terms make up the given output. The P term is the proportional gain times the error of that particular loop and the I term is the

integral gain times the sum of error since the PID controller was started. Hence, in mathematical form we have

$$output = K_p \cdot error(t) + K_i \int error(\tau) d\tau .$$

In the application of scanning a plate, the I term handles small error as a function of time and the P term handles large errors. The current code of the Arduino that processes the feedback loop can be seen in Appendix A.

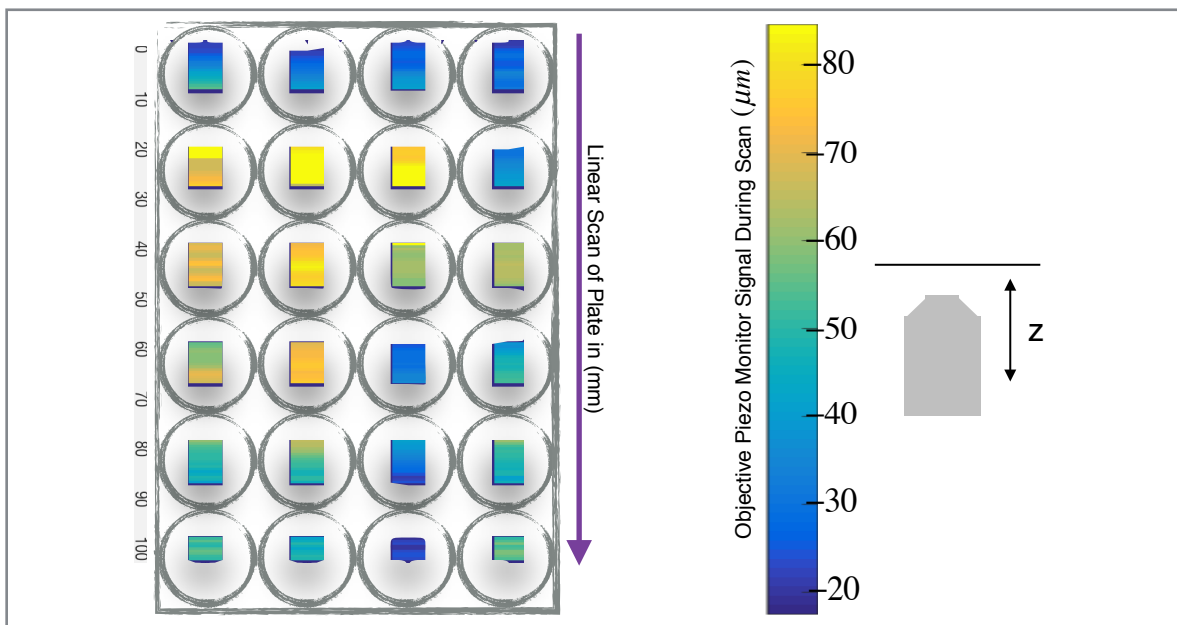


**Figure (2) Relative Objective Position for Typical Scan**

*The objective position in microns, showing the topography of a typical 24 well plate. Only the measurements of the forward scan are seen. This illustrates the need for an auto focus system if continues scanning is desired. To start each run, the objective is placed near the bottom of its 100 micron range to attempt keeping any fluctuations in the plate surface within the range of the piezo.*

In its current high speed set-up, at any magnification, the stage scans at a maximum velocity of 2mm per second while acquiring 4 frames, giving a spacing of one frame per .5 mm. The approximate time it takes the stage to make one pass across six samples covering a distance of 100 mm is 52 seconds. Once this pass is done, the data is saved to disk and the stage scans back through each well after a 1mm step in the

perpendicular direction. A video file with 210 frames is collected and parsed to the frames in the middle of each well. In this two minute span a 2x20 grid, in each well, is captured. The overall measurement and space between frames is dependent on the magnification. The spatial dimensions of the imaging grid can be seen in Figure (1-b,c). In Figure (1a) the normalized average pixel intensity of the interferogram per frame is plotted. One can see the peak intensity at the center of each well, where the frames used are chosen as those with an intensity at least 60% of the peak frames.

This faster imaging rate means the data will need to be processed faster. The capturing and logging of these videos are done with the capture computer (CC), and depending on the experiment at hand, will begin to scan for the next loop as soon as its finished. We want the CC to stay focused on the task that it has been given so all of the processing is done on another computer, the processing computer (PC). The PC is linked to the CC via a standard cat5 ethernet cord on a local network. This can be limiting depending on the desired turnaround time from capture to usable data considering the video file, for our current set-up, is approximately .5GB of data. If each video file takes 52 seconds to capture and write to disk, we can pull that file and start processing it right away. The parsing of the frames is done in one step where the video file is read from a disk on the CC and then written as a data file that contains an individual frame via the PC. Because this is done in real time, a custom Matlab code is needed to constantly compare the processed video files with the unprocessed video files. To ensure that the data files constructed from each video files are labeled correctly, the necessary location information is pulled from the video file first.

As each interferogram is pulled from the video file, it is converted into the flattened phase image before moving to the next. At the moment, this takes the most time. It takes approximately two second per frame to develop the phase image. Given this is

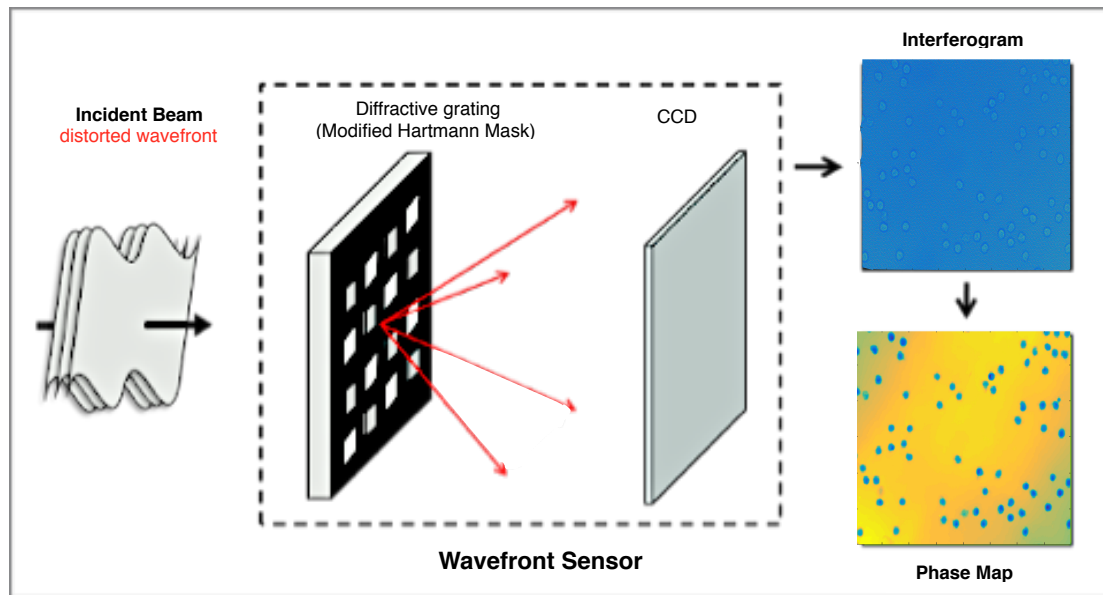


**Figure (3) Camera Technique**

*As the incident beam is diffracted by the grating, it is captured by the CCD sensor of the camera as a interferogram. It is then digitally processed to form the phase map for processing.(Bon, Maucort et al. 2009)*

most time consuming process, this is the only thing done during the experiment. The remaining process of tracking the cells is done after the experiment. The custom Matlab code first defines what is and what isn't a cell by a predefined range in both optical thickness and area. It can track the x and y position, mass and area of the cell, and compare the same metrics of the remaining frames from the same location. If these values don't vary more than a given threshold between frames, it is tagged and tracked as a cell.

The camera/interferometer used in the HSLCI set-up is a quadriwave lateral shearing interferometer (QLSI). This is label-free and provides additional phase information about the refractive index of each specimen. The refractive index distribution across the imaging plane creates contrast in the interferogram.

The advantage of a shearing interferometer is its self-reference capability. This allows for a simple and compact system that is not as sensitive to vibrations or other external noise. The interferogram is created by a diffractive grating mounted to the front of a CCD camera, where an incident beam is diffracted into four replicates. The replicas then interfere on the surface of the camera where the interferogram is recorded.

To get the unwrapped phase image, the intensity signal across the image matrix is deconvolved in the Fourier domain around the spatial period of the grating. This produces a phase gradient or map that is then numerically integrated to get the optical path difference. This is seen in Figure (3) where a simplified process of developing a phase map is shown.

The useful measurement made by the interferometer is the optical path difference(OPD) and is defined as a function of the spatial position in the wavefront. Thus

$$OPD(x,y) = \int_0^h [n(x,y) - n_{medium}] dz$$

Here  $n$  is the refractive index of the specimen and  $n_{medium}$  is the refractive index of the medium around it. The difference is integrated over the total thickness  $h$  in the direction

of propagation. This value is a combination of OPD from the specimen and the OPD from the imaging system, however we eliminate any contribution from the imaging system by subtracting the reference image captured before any measurements are made.

The OPD is then used to find the optical volume difference OVD, where the OPD is integrated over the total imaging surface. Hence,

$$OVD = \iint_S OPD(x,y) dx dy$$

This value is directly proportionate to the dry mass of the cell by a constant known as the specific refractive increment  $\alpha$ . The specific refractive increment is the rate of change in the refractive index  $n$  of a specific specimen. Therefore we have

$$\iint_S OPD(x,y) dx dy = \alpha \cdot m$$

This can be rearranged to find the mass;

$$m = \frac{1}{\alpha} S \cdot OPD$$

where  $S$  is the surface area of the specimen in microns. For the mass measurements

made during the current experiments  $\frac{1}{\alpha}$  is defined as  $5.56 \frac{pg}{\mu m^3}$ . (Reed, J. et al.

2011)

## Laser Focus Technique

The use of an optical beam deflection position measurement is used for a multitude of different scientific and commercial applications. There are many publications on different techniques to achieve reliable measurements. (Hsu, Lee et al. 2009, Liu, Lin et al. 2013, Xu, Liu et al. 2014) Most are concerned with the shape and density of the reflected beam because it is directly correlated to the noise in the optical signal. In Figure (4) you can see the general beam path used in the current set-up.

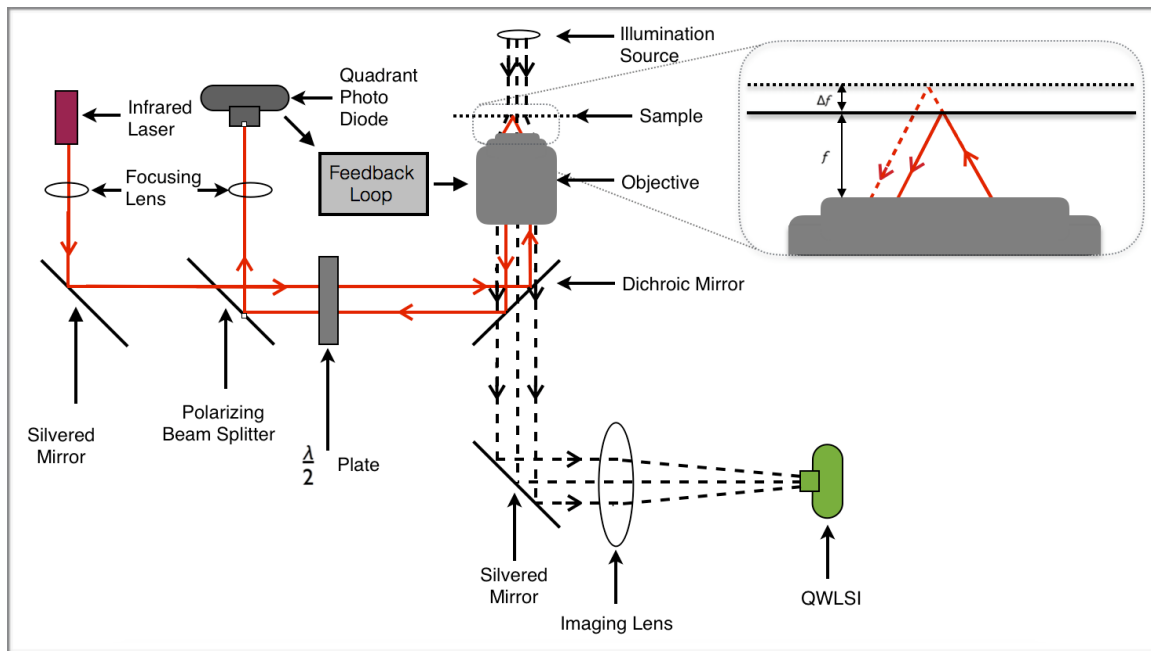


**Figure (4) Ray Diagram of Laser Focus System**

*A general arrangement of components for an optical beam deflection measurement can be seen.  $f$  is the desired distance from the objective to the water/glass interface. As the plate is moved across the objective, any change in this distance, denoted by  $\Delta f$ , is observed at the QPD.*

The laser used is a CPS980, by Thorlabs. The laser has a wavelength of 980 nm and produces an elliptical beam shape roughly 3.8 mm x 1.8 mm, with a power of 4.5 mW. It is particularly useful because it is compact at 11 mm in diameter and 40 mm in length



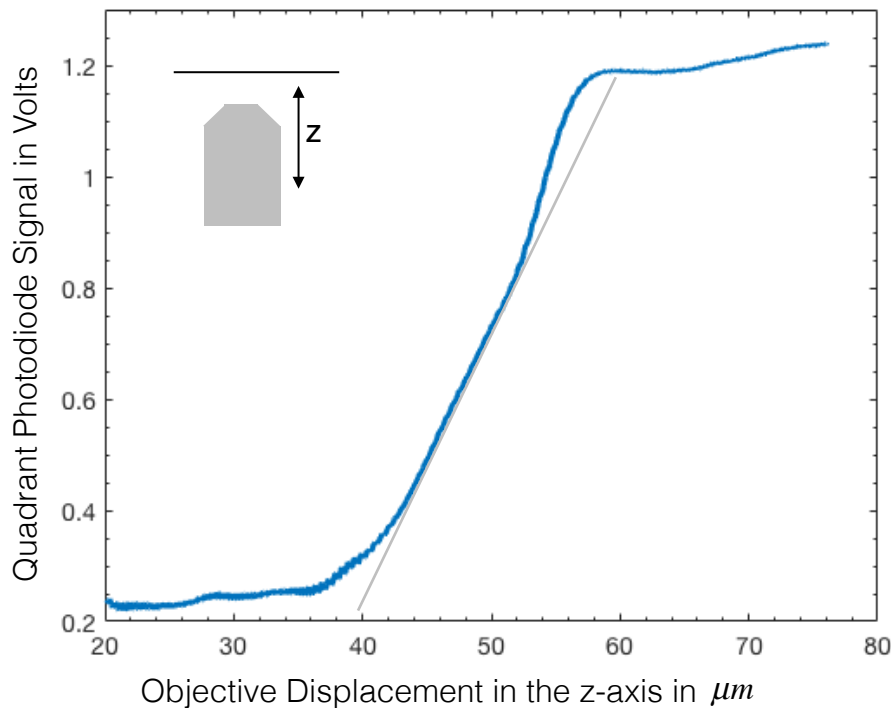
and is engineered to withstand large temperature variations. The laser is mounted into an adjustable mount so that the position of the beam incident on the rear aperture of the objective can be controlled. This can be adjusted to insure there is an offset of the laser beam from the optical axis.

The first lens the laser is passed through is a bi-convex lens with a focal length of 500 mm. It is placed roughly 100 mm in front of the laser and 305 mm from the sample. This helps to reduce the elliptical shape of the laser beam at the sample. Once the beam passes through the first focusing lens, it passes through a polarizing beam splitter where s-polarized light is reflected and p-polarized light is transmitted. In combination with the preceding half wave plate, this achieves two things. Since the laser diode has a polarization extinction ratio of 15 dB, nearly all of the laser is initially transmitted. The half wave plate is then used to rotate the polarization plane of the linearly polarized light. This is not as important for the beam from the laser as it is for the reflected beam. The wave plate can be adjusted so that the returning beam can be reflected instead of transmitted through the beam splitter. This reduces any interference that the returning beam may cause to the laser diode itself, as well as reflects it into the photo diode.

Once the beam is reflected off of the polarizing beam splitter, it is focused again with another bi-convex lens that has a focal length of 50 mm. This lens serves to control the spatial resolution of the distribution in the intensity of the laser beam. By adjusting the distance between the lens and the photo diode, you can mask any diffraction effects

from the different optical components. The spatial resolution of the diode is discussed in detail in its description later.

It is imperative to make any adjustments to the laser beam while the sample or water to glass interface is at the focal length of the objective as well as the piezo stack being in the middle of its range. There is a relative window where the displacement on the photo diode is linearly dependent on the distance between objective and sample. This window



---

**Figure (5) Objective Ramp vs. QPD**

*The semi-linear range in the middle of the graph is used as the dynamic range of the feedback input. The system typically stays within  $\pm 0.5 \mu m$  of the center as seen in Figure(9).*

---

is much greater than the focal range of the objective but fine adjustments can be made to ensure the reduction of noise over this range. When configuring, or taking a pre-run

quality check, the objective is made to ramp  $\pm 5\mu m$  to both insure quality and to find the ratio between photo diode signal and the displacement in micron of the objective. This is similar to figure (5) where the 40x objective is ramped  $\pm 30\mu m$  and the conditioned QPD signal in volts is plotted versus the displacement of the objective.

The key component in bringing together the laser optical path and the imaging path is a short-pass dichroic mirror with a cutoff of 805 nm. It spectrally separates any incident light by transmitting and reflecting it according to wavelength. Since the laser beam is in the near infrared range, 95% will be reflected. With the opposite effect, the imaging plane is transmitted allowing it to continue to the camera. The sample is illuminated with a 660 nm, 13 mW LED diode. The LED provides a spatially coherent light source that is optimal for the phase imaging process of the interferometer. When using higher magnification, a focusing lens is required to direct as much light into the objective as possible. Once the plane wave of the image passes through the dichroic mirror, they are focused with an imaging lens into the camera.

# Electrical Circuitry/Hardware Interfacing

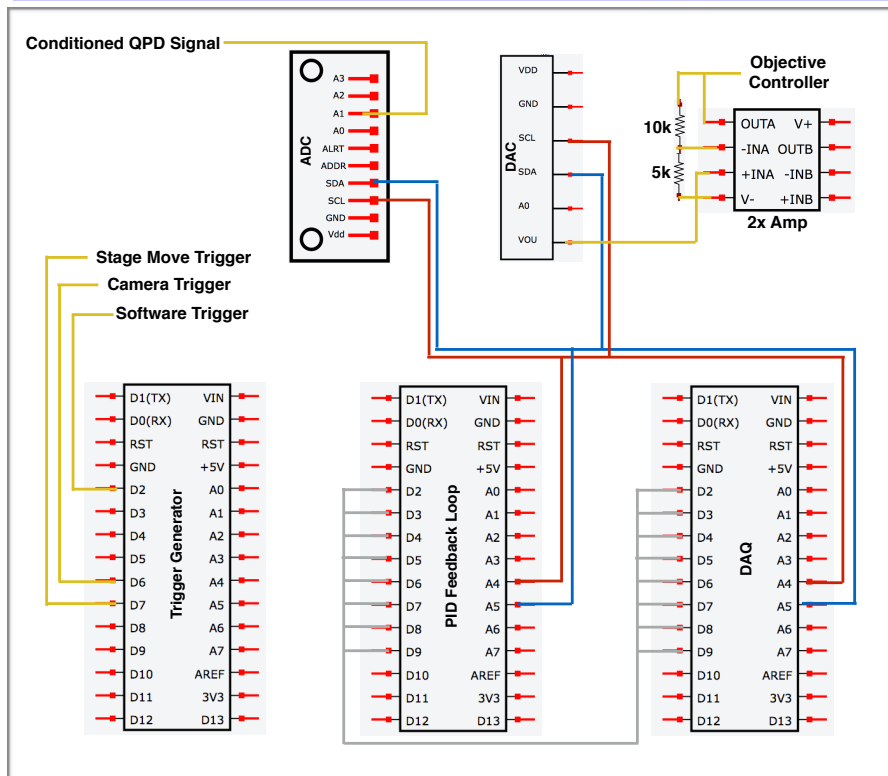
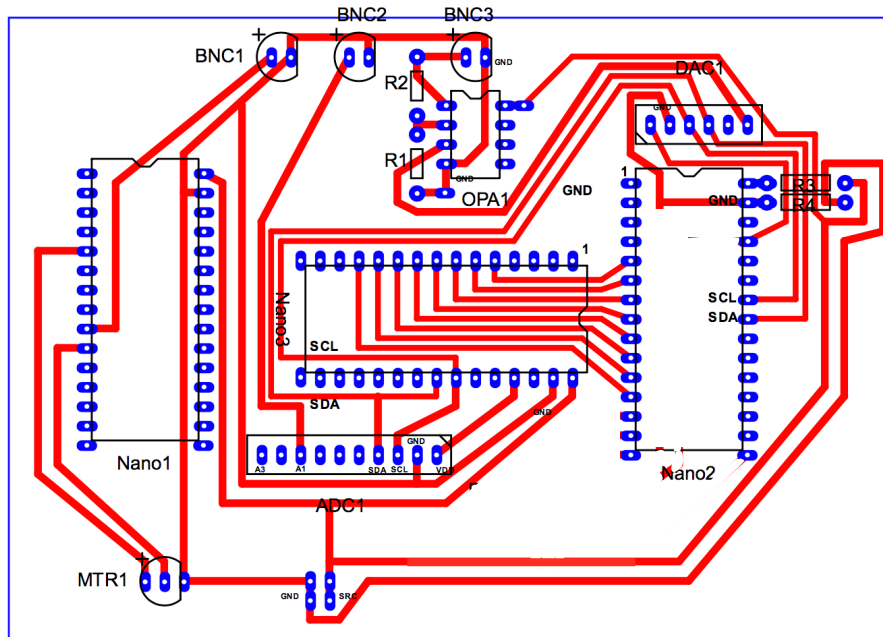


**Figure (6) Layout of Circuit**

(a) PCB board designed in current configuration. (b) Simplified layout of circuit that shows the connections of all data signals.

The idea in designing a commercial or scientific device is to find the balance between the cost and efficiency of the electronic circuitry or hardware. Today's "open source" market offers a number of different options.

In Figure (7), each component with the communication type and direction associated with it is shown. The user interface is done in the numerical computing environment MATLAB. Each device that is linked to MATLAB uses an existing driver that allows easy use of MATLABs functions.

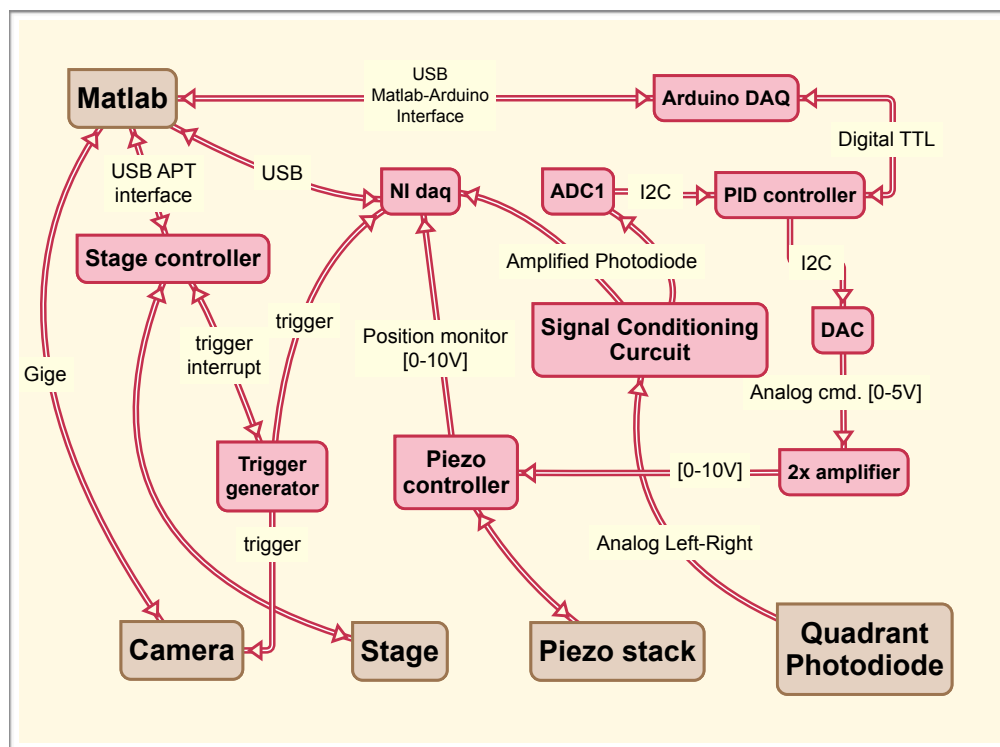


**Figure (7) Hardware Configuration**

*The type and direction of each communication path is shown.*

The interferometric camera uses the GigE Vision interface that is based on the Ethernet standard. With this connection, images/videos can be transferred from the camera to the CC at a rate up to 10 Gbits/s, but currently the 1GigE version is being used. The

main difference in GigE Vision and other internet protocols is that a point-to-point connection is created to avoid interaction from external devices. This means that the user must configure the device, instead of automatic configuration found in other protocols. This allows for a faster transfer rate and higher bandwidth. The camera is configured to receive a trigger signal that controls the fps. This is done with an Arduino nano, where the stage move trigger is configured to an interrupt pin on the nano to insure that the stage and camera are always in sync. At the end of each pass the video file is save to disk and the camera is set-up for the next acquisition.

The motors that control the x, y, and z motions of the stage are linked to MATLAB via a USB COM port to a Thorlabs APT stepper motor controller. This controller uses a digital signal processor (DSP) and the ActiveX software framework to give high resolution micro-stepping. Like other in-process COM servers the Thorlabs APT ActiveX control is used as the server and MATLAB is a control container or client. Therefore both a GUI and MATLAB scripts can manipulate the ActiveX controls' properties, methods and events. The motors are linked to the controller through 15-pin D-sub connectors that allow for encoding and 48V 2-phase bipolar motor outputs. The controller is also connected to the trigger generator with a 5V logic level output that generates a signal when the stage begins to move.

For the purpose of high bandwidth data signal acquisition and error analyses, a NI USB-6002 DAQ is connected to MATLAB using the MATLAB data acquisition toolbox. Using a session-based interface, a binary file including the camera trigger, amplified

photo diode signal and position monitor of the piezo stack are saved to disk to accompany each video file.

The last component that is directly linked to the MATLAB interface is the Arduino DAQ. This uses a MATLAB support package that uses a server program running on the board to execute and receive commands via a serial port. This is a necessary connection between the PID controller and MATLAB for a number of reasons. The PID controller could not be directly connected because the support package only allows for control loops to run at up to 25 Hz. This is much slower than the capabilities of the Arduino and thus dramatically slowing down the refresh rate of the feedback loop. As the PID controller is the only thing controlling the position of the piezo, handshaking is done to go between ramp and PID functions. In addition to function switching the PID controller sends a signal to MATLAB via the Arduino DAQ that the piezo stack is at the top or bottom of its range. This then causes the stage to step in the z-direction to bring the piezo back into its operating range. This can be seen in Figure (2) where the piezo reaches the top of its range and is suddenly shifted by 35 microns. The handshaking that is done between the Arduino DAQ and PID controller is achieved with multiple digital pins using TTL type logic.

The PID controller is solely designed to process the input signal and define an output. Because the Arduino Nano has limitations in voltage range and resolution, the I2C bus line built into the Arduino is used to communicate with additional breakouts. The input signal from the photodiode sensor has a range of  $\pm 15$  V so a signal conditioning circuit

is needed to convert the signal into the desired range of [0-5V]. The analog input resolution for the Arduino nano is 8-bits where a higher resolution of 16-bits was accomplished by using the ADS1115 analog to digital converter (ADC) breakout made by Adafruit industries. This breakout is capable of 860 samples per second over the I2C bus line and only consumes 150 micro-amps of energy. On the same bus line, the MCP4725, a 12-Bit digital to analog convertor (DAC) also made by Adafruit. is used to give a output voltage range from [0-5V]. The Arduino has built in ADCs on their analog pins, but the nano does not contain a DAC. Therefore the ADC was a bonus addition to the set-up while the DAC is more of a necessity. Downstream from the DAC is a 2x amplifier comprised of an op amp and two resistors. This brings the output voltage of the feedback loop into the [0-10V] range that the piezo controller is expecting.

The piezo controller that was used was a *Nano-Drive*<sup>®</sup> and the piezo stack was a Nano-F100S, both by Mad City Lab. The controller runs in a closed feedback loop with the stack to ensure that the relationship between the input voltage and displacement of the piezo remains linear. This gets rid of any creep and hysteresis found in piezo actuators. The piezo stack uses internal position sensors to keep the error in linearity, over the full range, to  $\leq 0.01\%$ . The [0-10V] input is mapped directly to a [0-100  $\mu\text{m}$ ] range at the objective.

The optical beam detector that was used was a Thorlabs PDQ80A quadrant position detector. This sensors peak responsivity is at 900nm which is in the IR range of our laser. The recommended laser spot size for this sensor is 1-3.9  $\text{mm}$   $\varnothing$  to ensure that you



don't lose a significant amount of signal strength when the spot crosses the  $\sim 1 \text{ mm}$  gap between any quadrant. This sensor is very sensitive to the shape and density distribution of the incident beam. As seen in the ray diagram, a series of lenses were

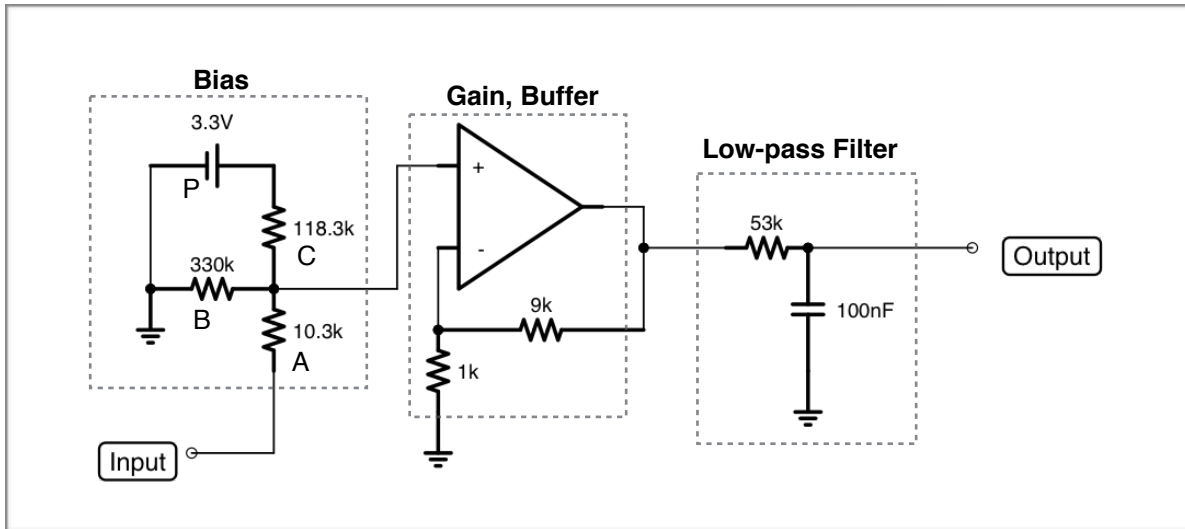


**Figure (8) Instrumentation Amplifier Diagram**

A series of components are needed to construct a reliable QPD signal. This figure shows a signal processing schematic using a series of resistors, op amp, and capacitor.

needed to minimize diffraction patterns (from the glass thickness of beam splitters and the dish itself) in the beam. If the beam is not focused to a small spot, the diffraction patterns will dominate during a ramp of the piezo stack. Essentially the beam needed to be focused down to the point where the distance between each peak was smaller than the resolution of the diode. This gives a beam, whose distribution within the beam as well as the beam, moved side to side. The final desired beam size was measured at  $\sim 0.75 \text{ mm } \varnothing$ .

The change in voltage coming directly out of the QPD during a  $\pm 5 \mu\text{m}$  ramp is  $\sim \pm 25 \text{ mV}$ .

Therefore to condition and amplify the signal an instrumentation amplifier was used. As seen in Figure(8), there are a multiple components that make up the amplifier. The gain/

buffer is accomplished with a standard op-amp circuit where the gain is set by the two resistors and the buffer range is set by the powering voltage. The low-pass filter seen has a attenuation of 6 dB at 30Hz. This can be adjusted to accommodate any noise coming from the electronics or environment. The biasing circuit is a bit more complicated. Once the voltage range coming out of the QPD is found, the following equations can be used to find the needed values of the resistors A, B, C and secondary power supply P;

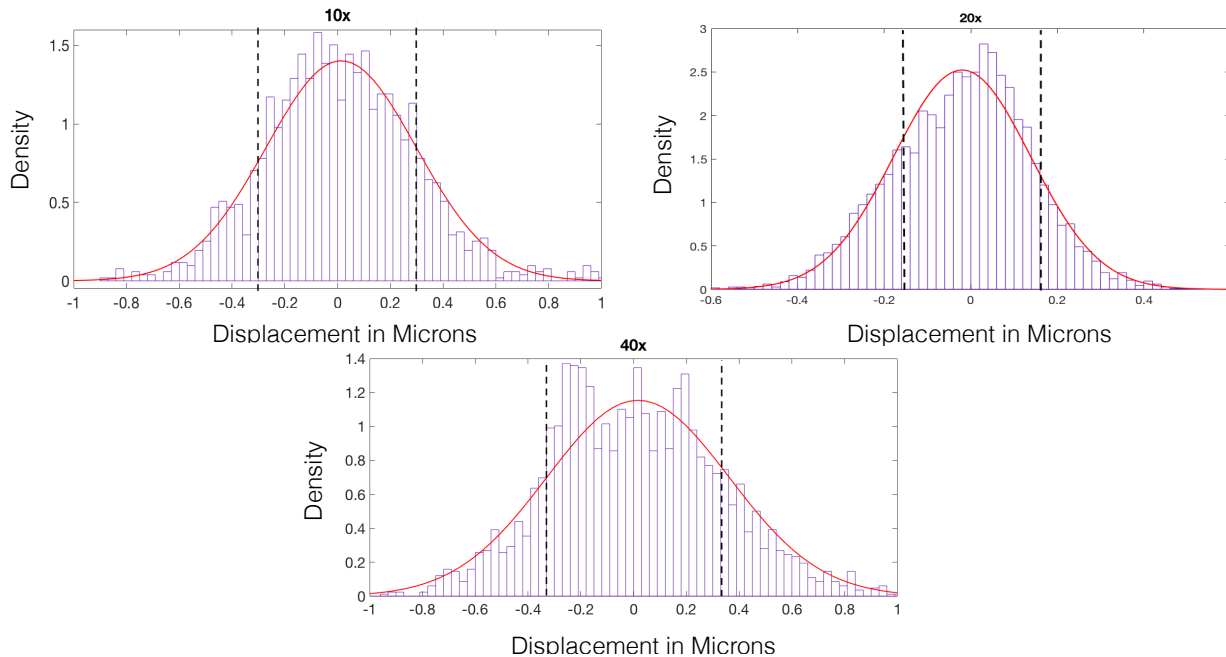
$$(G - 1)a + Gb + Gc = 0$$

$$Ma + Mb + (M - P)c = 0$$

G is the gain defined as the change in output over the change in input  $\frac{dOut}{dIn}$ , M is the midpoint of the desired output range, and a, b, c are the inverses of A, B, C. In order to solve the equations a third equation is needed and can simply just define one of the resistors such as  $a = 1/10.3k$ . The biasing circuit shown takes a  $\pm 25mV$  centered at 0V and brings it up to a  $\pm 250mV$  centered at  $\pm 250mV$ .

# Validation

## PID Error



---

### **Figure (9) Histograms of Error**

*For each magnification, a series of 20 loops down one column of wells was performed.*

*The density of QPD displacement signals from optimal focus is plotted. The dashed lines show the standard deviation calculated for the given data set.*

---

To analyze both the error and piezo position signals, a NI USB-6002 was spliced into the signal processing network. The camera trigger was also captured so that the data could be filtered down to just the data during the exposure time of the camera. If only one analog input is being acquired, the NI DAQ can acquire at a maximum sample rate of 50kHz. However there were three analog signals acquired so that gave a maximum sample rate of 15kHz. If the camera exposure time is 500 micro seconds, then the interesting data points would be eight data points past the rise in trigger. Using custom Matlab code, the eight data points were averaged and a data set of 210 averaged data

points was formed for each run. Then, in a similar manner to the logging of camera frames, this is appended to each frame. Figure (9) shows the histograms developed after 20 loops for each magnification. The depth of field varies for each and is as follows;

$$\begin{array}{l} 10x \approx \pm 5 \mu m \\ 20x \approx \pm 3 \mu m \\ 40x \approx \pm 0.5 \mu m \end{array}$$

The feedback was able to keep the standard deviation within these ranges. Because the same sensitivity is achieved for each magnification, the standard deviation is comparable for each.

## Effect of temperature

During the majority of the run, temperature fluctuations is not a concern because the system is kept in an incubator at a constant  $36^{\circ}\text{C}$ . However, when a line of cells is to be treated, the incubator is opened for approximately one minute. Therefore a test was performed where the feedback loop was on while the incubator door was held open to resemble a time lapse of treatment. If the feedback loop was to be tracking during this time, then any fluctuations in the system would be absorbed and the images should stay in focus.

The test was successful at capturing any fluctuations in the system. There was a drop in temperature of about  $.6^{\circ}\text{C}$  and no significant fluctuations in focus. The piezo monitor signal was captured and a  $6\ \mu\text{m}$  step was needed to stay in focus. This means that, with in a respectable range, there is a dependence on temperature for the distance the plate is from the objective. After repeating an identical test, an average dependence was found at  $10\ \mu\text{m}$  per  $^{\circ}\text{C}$ .

There could be many factors that contribute to the sensitivity of the system to temperature. There are multiple stages stacked on top of each other as well as the glass that makes up the bottom of the dish can shrink and sweep as well. Overall any affects from a change in temperature are washed because the interface that is used for focusing is not going to change.

## Mast Cell Experiment

### Design of experiment

Mast cells are the front line defense against pathogens and allergens in the body. They are used to trigger inflammation that helps to increase blood flow and vascular permeability. In order for the mast cells to achieve this, the pathogens activate the mast cell to release stored histamine. This process is called degranulation.

The direct advantage of the high speed system to the mast cell experiments was its ability to acquire a lot of data in a useful amount of time. On average, 10-15 cells are found in each frame at 40x. Therefore with the HSLCI, if we capture almost nine times the amount of frames for each the control and treated samples we will get enough cells to develop a good distribution of masses.

$5 \times 10^5 m L^{-1}$  cells, media, and  $200mM$  dinitrophenylated human serum albumin (DNP-HSA) the triggering chemical, are acquired before the beginning of each run. Each run of the experiment was kept to one column of six wells, with a reference well on the opposite end of the 24 well plate. For each run the control and treated wells were alternated to keep any traits inherent to the HSLCI from affecting the data. Once the cells were plated, they were carried to the HSLCI incubator that was already at the desired CO<sub>2</sub> and temperature levels. After 30 minutes of resting time for the cells, the experiment was started. For the first hour, or 30 runs, the HSLCI ran as fast as possible to get a good baseline for the current batch of cells. Next, the designated treated wells were given  $12.5 \mu L$  of DNP-HSA and the system was immediately started back into

acquisition. For the next hour the HSLCI was run at the same time resolution so that it could capture the degranulation process. Once the second hour was finished the system slowed down the acquisition to a new frame every 20 minutes for the next 48 hours. During this time the incubators temperature and CO<sub>2</sub> levels were closely monitored to insure stability.

## Results

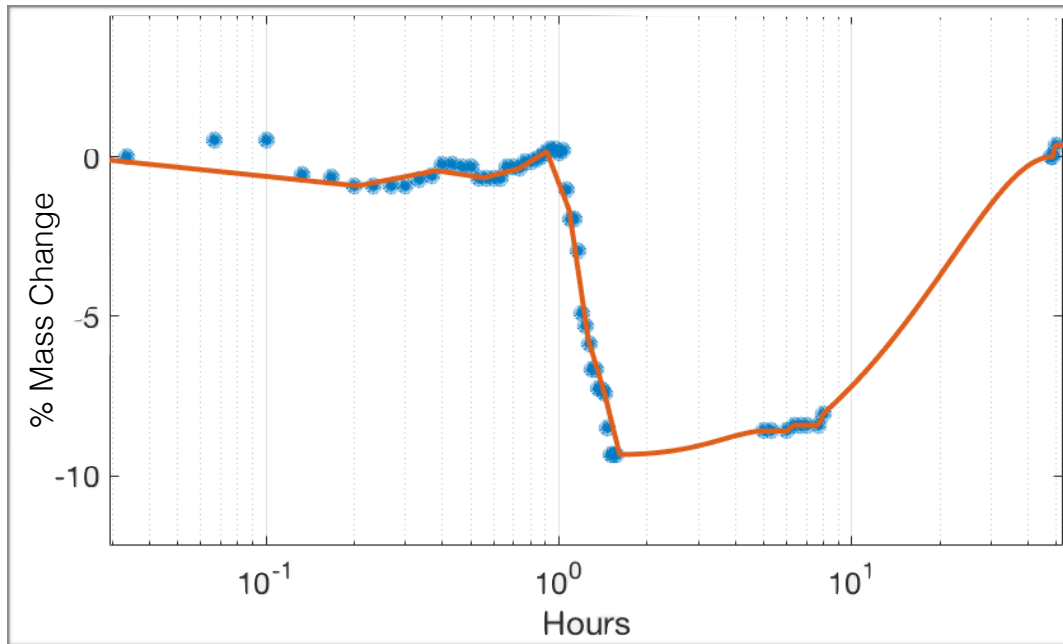


**Figure (10) Mast Cell Mass Track**

*The typical percent difference between a control and treated well. The treated well is the baseline for the calculations shown. After the first two hours, only the data points right after stirring are shown.*

The design of the imaging grid proved useful when trying to average a large number of different mast cells. For the wells used in Figure (10), as well as the remaining wells, an average of 700 cells were captured per well for each loop. The imaging grid created a scanning strip down the center of each well. Because each 24 well plate is roughly 100 $\mu\text{m}$  higher in the center, the cells in each well moved in synchrony where the direction was determined by the gradient of the bottom of each well. This is dictated by the wells location relative to the center, i.e. the cells eventually line the outer edge of the plate. Because of this, the average mass measurement for each well would decline exponentially after approximately 5 hours. To remedy this, the wells were stirred, using a 1000 $\mu\text{L}$  pipet that was replaced for each well to avoid any cross contamination. The



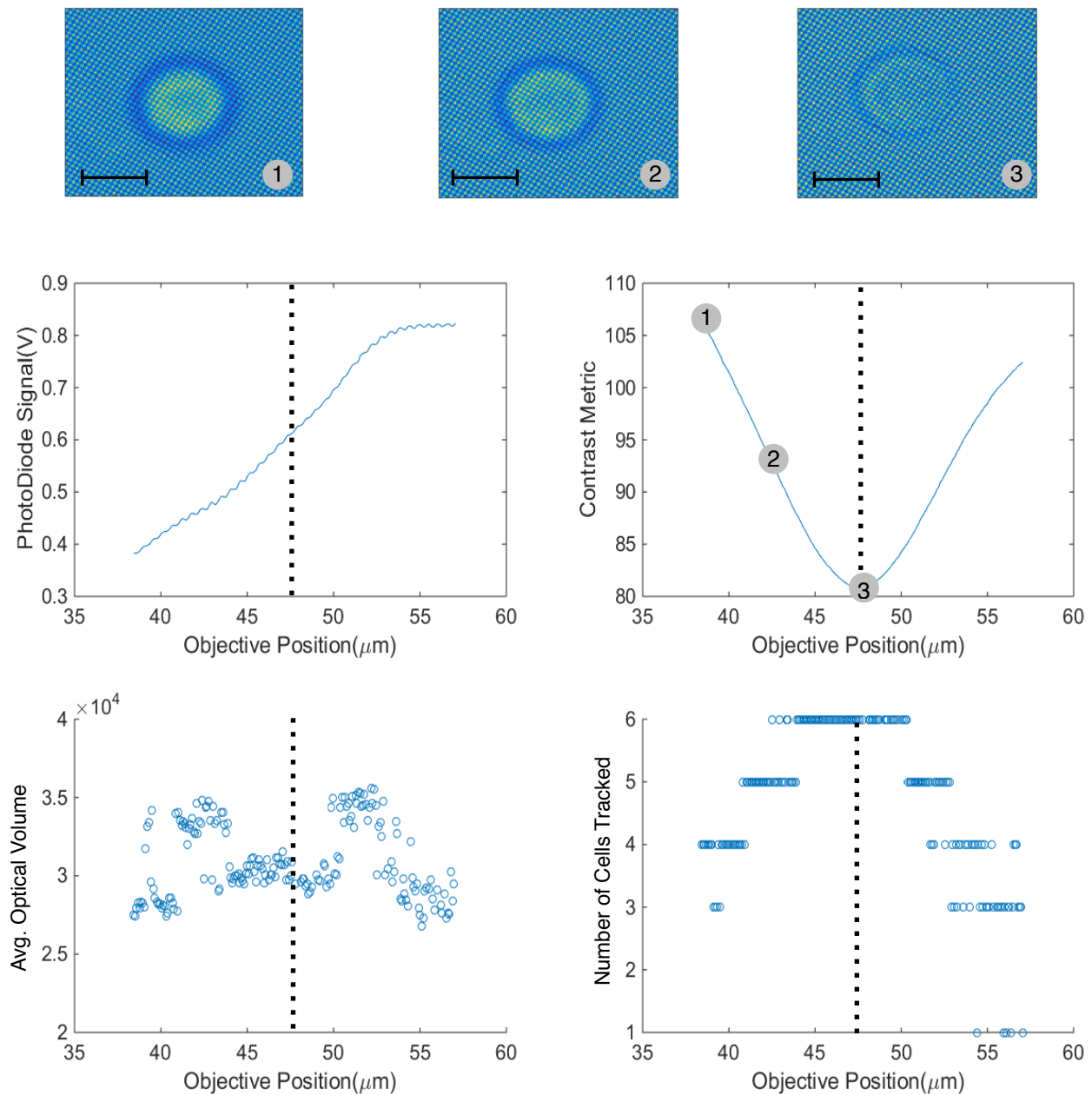


**Figure (11) 20 μm Ramp @ 40x**

*This figure shows the relationship between the objective position and various metrics used in parameterizing the mass measurements of the mast cells. A region, including one tracked mast cell, has been selected to show resolution and contrast as the objective is moved through focus. The scale bar on the selected images represents 10 μm and the dotted lines represent the objective position of best focus.*

cells were pipetted twice, while moving around the well to insure that an even distribution was re-established. This proved to be the only step necessary, because the average mass measurements would fall right back into line with the previous track it was making. This regain in measurement stability allows us to omit the measurements where the mass is declining.

Because a large distribution of cells are seen each loop in each well, there were small fluctuations in the mass measurements. This is remedied by calculating the difference between treated and non-treated wells. Figure (10) shows that after 48 hours there was no difference in treated and non-treated. This is not the time that the treated well took to regain the mass it lost, but the time it took for the treated to catch up with the non-treated. For the initial hour, all of the wells gained approximately %5 mass. From that point on the non-treated wells continued to gain another %10 over the next 48 hours.

For quality control, it was useful to determine the effects that focus position had on the mass measurements. In Figure (11), multiple metrics were plotted while a  $20\mu m$  ramp was performed. The contrast metric seen is found using a filter that determines the overall contrast of the image by comparing the difference in neighboring pixels. The objective position that gives the least contrast is the position of best focus is found at approximately  $47\mu m$ . This can then be compared to the remaining metrics where we see a definite relation. In this particular frame one can see that, while in focus, six cells are trackable. There is a range of  $5\mu m$  that all possible cells are seen with little

variation in mass. This range is much larger than the range seen in Figure (10) where the standard deviation of the error signal, during an entire experiment at 40x, is  $0.34\mu m$ .

## Possible addition to experiment

The next step, if found useful, is to see how long before they can be re-triggered. This would be particularly useful to the immunology community because this could give a metric on the effectiveness or reproducibility of the immune system. The need for stirring can be remedied by causing the entire apparatus inside the incubator to pivot in the x and y directions. This can be done to overcome the gradient of the bottom of each well. Given the data is processed in real time, a feedback loop comparing the velocities of the cell could be used for the entire duration of the run. This would insure that the plate of cells would only be disturbed when the trigger is administered.

## **Conclusion**

In conclusion, it has been shown that the addition of laser autofocus to existing live cell interferometric measurements allows for an increase in data and time resolution. The technique is low-cost and can be introduced to any scanning microscopy applications. The necessary technique is shown in detail and can be reproduced to fit the end users needs.

## Appendix A

```
// Define variables used throughout
float Kp = .06, Ki = .096, Kd = 0, errorsum = 0; //PID gain value
float SensorSignal, SetPoint, SensorValue;
float error, PiezoCmdSignal;
float Focus_Signal, k, resetValue, Setpoint, sigDifference;
float PIDValue, RampValue, SetPointValue;
float Pout, Iout, Dout, Output; //PID final output variables
float multiplier = 0.3125F;

//Range in 12-bits of DAC
int Mid = 1950, Min = 0, Max = 3900;

// Define digital pins
int Sensorpin = A2, Outputpin = 4, x = 5, moveMotor = 0, triggerValue = 0, PIDstartValue = 0;
int PIDPIN = 8, RampPIN = 7, SetPointPIN = 6, ResetPIN = 4;

int MoveUpPIN = 9, MoveDownPIN = 5, moveupStat = 1, movedownStat = 1;

int DELAY = 0;

#include <avr/interrupt.h>
#include <Wire.h>
#include <Adafruit_MCP4725.h>
#include <Adafruit_ADS1015.h>
#include <SPI.h>
Adafruit_MCP4725 dac;
Adafruit_ADS1015 ads;
#define DAC_RESOLUTION (12)

void setup() {

  pinMode(2, INPUT); // interrupt input
  //attach our interrupt pin to it's ISR
  attachInterrupt(0, enableISR, FALLING);

  // we need to call this to enable interrupts
  interrupts();
  enable = 0;
  Serial.begin(9600);

  Wire.begin(8);
  Wire.onReceive(receiveEvent);
  pinMode(Outputpin, OUTPUT);
  pinMode(PIDPIN, INPUT);
  pinMode(SetPointPIN, INPUT);
  pinMode(RampPIN, INPUT);
  pinMode(MoveUpPIN, OUTPUT);
  pinMode(MoveDownPIN, OUTPUT);

  // The ADC input range (or gain) setting
  ads.setGain(GAIN_FOUR); // 4x gain +/- 1.024V 1 bit = 0.03125mV

  dac.begin(0x62);
  ads.begin();
}
```

```

// The interrupt hardware calls this when we detect pulse
void enableSR() {
  enable = 1;
}

void loop() {
  SetPointValue = digitalRead(SetPointPIN);
  RampValue = digitalRead(RampPIN);
  PIDValue = digitalRead(PIDPIN);

  //used to find set-point value of focused frame
  if (SetPointValue == 1 && PIDValue == 0 && RampValue == 0)
  {
    SensorValue = - ads.readADC_Differential_0_1() * multiplier;
    Serial.println(SensorValue);
  }

  //PID function
  else if (SetPointValue == 0 && PIDValue == 1 && RampValue == 0)
  {

    Setpoint = 4400;//4950 40x

    SensorValue = -ads.readADC_Differential_0_1() * multiplier;

  //Check for erratic behavior
  error = Setpoint - SensorValue;
  if (error >= 2000)
  {
    SensorValue = Setpoint;
  }
  error = Setpoint - SensorValue;

  errorsum = errorsum + error; // add curent error to running total of error

  //Check windup
  if (errorsum >= 170000) {
    errorsum = 0;
  }
  // calculate PID gains

  Pout = Kp * error;
  Iout = Ki * errorsum ;

  PiezoCmdSignal = (Pout + Iout) + Mid; // prep the output variable

  //Check if stepper motor is being moved
  if (enable == 1)
  {
    PiezoCmdSignal = Mid;
  }
}

```

```

enable = 0;
moveupStat = 0;
movedownStat = 0;

if (PiezoCmdSignal >= Max)// sanity check of the output, keeping it within the
{
  movedownStat = 1;
  PiezoCmdSignal = Max; // available output range
}

if (PiezoCmdSignal <= Min)
{
  moveupStat = 1;
  PiezoCmdSignal = Min;
}

delay(1);

dac.setVoltage(PiezoCmdSignal, false);

digitalWrite(MoveUpPIN, moveupStat);
digitalWrite(MoveDownPIN, movedownStat);

} // end if (PIDSwitchpin == HIGH)

//Ramp function
else if (SetPointValue == 0 && PIDValue == 0 && RampValue == 1)
{

  int Max_Ramp = Mid + 0.05 * Max;
  int Min_Ramp = Mid - 0.05 * Max;
  for (int i = Mid; i < Max_Ramp; i = i + x) {
    if (i > Max_Ramp)// sanity check of the output, keeping it within the
      i = Max_Ramp; // available output range
    Focus_Signal = i;
    delay(DELAY);
    dac.setVoltage(Focus_Signal, false);
    SensorValue = - ads.readADC_Differential_0_1() * multiplier;
  }

  for (int i = Max_Ramp; i > Min_Ramp; i = i - x) {
    if (i < Min_Ramp)
      i = Min_Ramp;
    Focus_Signal = i;
    delay(DELAY);
    dac.setVoltage(Focus_Signal, false);
    SensorValue = - ads.readADC_Differential_0_1() * multiplier;
  }

  for (int i = Min_Ramp; i < Mid; i = i + x) {

```



```

    if (i > Mid)
        i = Mid;
    Focus_Signal = i;
    delay(DELAY);
    dac.setVoltage(Focus_Signal, false);
    SensorValue = - ads.readADC_Differential_0_1() * multiplier;
    }
    delay(DELAY);
} // end if (RampSwitchpin == HIGH)

else
{
    dac.setVoltage(Mid, false);
    digitalWrite(triggerPIN, 1);
    l = 0;
    error = 0;
    errorsum = 0;
    delay(10);
}
}
} // end void loop()

//this function is used to update PID parameters via I2C if needed
void receiveEvent(int howMany) {
    while (1 < Wire.available()) { // loop through all but the last
        char c = Wire.read(); // receive byte as a character
        delay(10);
        switch (c) {
            case '1': //byte a; byte b; byte c; byte d; byte bytes;
                { int x = Wire.read(); // receive byte as an integer
                    float y = x / 100;
                    float z = x % 100;
                    float h = y + z / 100;
                    //Serial.print(y); Serial.print(" "); Serial.print(z); Serial.print(" "); Serial.println(h);
                    Kp = h;
                }
                break;
            case '2': //byte a; byte b; byte c; byte d; byte bytes;
                { int x = Wire.read(); // receive byte as an integer
                    float y = x / 100;
                    float z = x % 100;
                    float h = y + z / 100;
                    //Serial.print(y); Serial.print(" "); Serial.print(z); Serial.print(" "); Serial.println(h);
                    Ki = h;
                }
                break;
        }
    }
}
}
}

```

## Bibliography

- Bon, P., G. Maucort, B. Wattellier and S. Monneret (2009). "Quadriwave lateral shearing interferometry for quantitative phase microscopy of living cells." Opt Express **17**(15): 13080-13094.
- Hsu, W. Y., C. S. Lee, P. J. Chen, N. T. Chen, F. Z. Chen, Z. R. Yu, C. H. Kuo and C. H. Hwang (2009). "Development of the fast astigmatic auto-focus microscope system." Measurement Science and Technology **20**(4).
- Liu, C. S., Y. C. Lin and P. H. Hu (2013). "Design and characterization of precise laser-based autofocusing microscope with reduced geometrical fluctuations." Microsystem Technologies-Micro-and Nanosystems-Information Storage and Processing Systems **19**(11): 1717-1724.
- Reed, J., Chun, J., Zangle, T., Kalim, S., Hong, J., Pefley, S., Zheng, X., Gimzewski, J., Teitell, M., (2011) "Rapid, massively parallel single-cell drug response measurements via live cell interferometry." *Biophys. J.* 101, 1025–1031
- Xu, H., J. Liu, Y. Li, Y. Yin, C. Zhu and H. Lu (2014). "Autofocus using adaptive prediction approximation combined search for the fluorescence microscope in second-generation DNA sequencing system." Appl Opt **53**(20): 4509-4518.